International Journal of Clinical Images and Medical Reviews

ISSN 2771-6309

Research Article

Digital phantoms for evaluating the dosimetric Impact of MRI Geometric inaccuracy in SBRT planning for liver cancer in the presence of motion

Tarraf Torfeh*, Rabih Hammoud, Amine Khemissi, Souha Aouadi, Satheesh Paloor, Noora Al-Hammadi

Department of Radiation Oncology, National Center for Cancer Care & Research (NCCCR), Hamad Medical Corporation, Doha, Qatar.

Abstract

MRI is increasingly being used in radiotherapy applications for tumor delineation and tracking in the presence of respiratory motion. The purpose of this work is to investigate the impact of system-related MR geometric inaccuracies on dose distributions for liver stereotactic-body radiation therapy (SBRT) using digital phantoms.

A methodology of generating digital phantom was developed and presented in this study. Based on this methodology, two types of digital phantoms were generated. The first type is composed of 3D shapes with well-known geometry while the second type is extracted from CT patient images. These digital phantoms were then deformed based on a previously calculated distortion map. Highly conformal volumetric (VMAT) modulated arc therapy plans were then optimized on the distorted dataset and transferred to the original dataset and dose distribution was analyzed.

Dosimetric evaluation on these digital phantoms showed that the dose received by the original set of images was higher than the dose received by the distorted images. Results also showed that the difference in the DVH is inversely proportional to the target size.

The methodology used in this study, represents an important technique allowing the assessment of the dosimetric impact of organ deformation for different anatomic sites as well as treatment techniques.

Keywords: digital phantoms, MRI distortion, dosimetric impact, SBRT.

Introduction

Recent advances in radiation therapy have placed Stereotactic body radiation therapy (SBRT) as a superior therapeutic option for the treatment of various tumors especially in the liver compared to other RT techniques [1 - 5]. SBRT has shown a sustain improvement of local control rates of tumors that are subject to motion. However, precise delineation of patient anatomy is required due to the sharper dose fall-off at the edge of target in Volumetric Modulated Arc Therapy (VMAT) plans used with SBRT.

On the other hand, due mainly to its superior soft tissue contrast compared with computed tomography (CT), data from magnetic resonance imaging (MRI) is increasingly being used for radiation therapy. MRI-only based dose planning for external beam radiation therapy has been increasingly gaining research interests and some commercial solutions has been already proposed and adopted [6, 7]. The main reason behind this interest resides in the fact that the current planning of radiotherapy treatments which combines MRI and CT through image registration has several drawbacks such as the registration, the irradiation dose to the patient from CT and the time allocated.

Consequently, MRI represents a promising technology and alternative to the four-dimensional computed tomography (4D-CT) to assist in volume contouring for external beam radiation therapy. As such, motion management strategies based on MR only images have been proposed lately [8-19].

One of the main obstacles to using MR image sets in the design of motion management strategies is the existence of system-related geometric inaccuracies caused mainly by the inhomogeneity in the main magnetic field and the nonlinearities of the gradient coils.

The dosimetric impact of MRI system-related inaccuracies has been evaluated and reported in the literature [20-35]. These evaluations were performed using either images issued from real patients or images issued from digital phantoms. However, all of these studies treated the dosimetric impact of MR inaccuracies in static mode and none has included the motion factor.

In this current work, we present a methodology for the development of digital phantoms used in order to investigate the dosimetric impact of MR system- related inaccuracy during motion on treatment plans in an MR-only workflow. MR distortion maps as well as blurring artifacts calculated in our previous work [36] were used to deform different type of digital phantoms. Dose plans were initially generated and optimized on the distorted datasets and then transferred to the original datasets to calculate new dose distributions and to study the MR geometric inaccuracy impact on dose–volume histograms (DVHs).

***Corresponding Author:** Tarraf Torfeh, Ph.D,Department of Radiation Oncology, National Center for Cancer Care and Research, NCCCR Hamad Medical Corporation, Doha, Qatar

Received: July 19, 2022 **Published:** July 28, 2022

Citation: Tarraf Torfeh*, Rabih Hammoud, Amine Khemissi, Souha Aouadi, Satheesh Paloor, Noora Al-Hammadi. Digital phantoms for evaluating the dosimetric Impact of MRI Geometric inaccuracy in SBRT planning for liver cancer in the presence of motion. Int Clin Img and Med Rew. 2022; 2(4): 1087.

***DOI:** 10.55920/IJCIMR.2022.02.001087*

Materials and Methods

MR geometric accuracy measurement

The MR geometric distortion as well as blurring artifacts during motion presented in this study were measured and reported in our earlier study [36]. In that study, Axial, sagittal and coronal Cine MR slices acquisitions of an in-house motion phantom were compared with the CT images using our in-house developed software.

3D distortion map was then produced and blurring artifact was assessed by measuring the Full Width at Half Maximum (FWHM) of the control points.

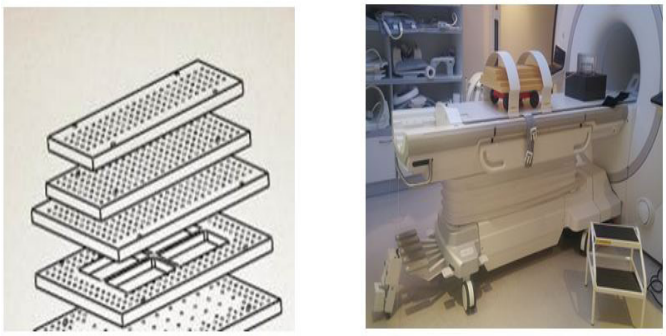

Figure 1: *a) View of the phantom showing the layers and b) the Phantom placed on a track attached to the motion motor positioned inside the MR.*

Dataset

Digital phantoms composed from 3D shapes

Using in-house software, 3D digital phantoms were created using different 3D shapes including spheres, ellipses and cylinders as shown in figure 2.

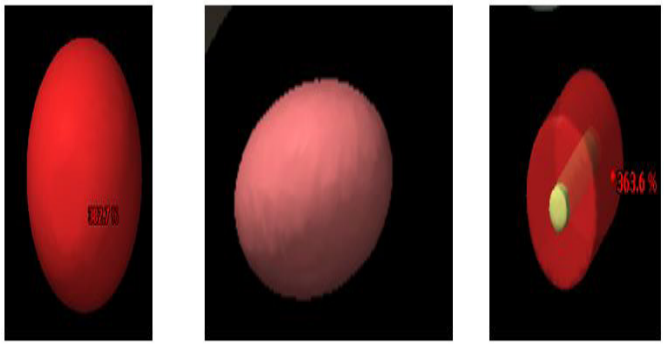

Figure 2: *Different 3D shapes used to create digital phantoms*

A dataset of 2D images was then generated from these digital phantoms as shown in figure 3. Based on acquisition parameters specified by the user such as slice thickness and pixel size, 2D acquisition planes were created and images were generated by calculating the intersection between these planes and the different 3D shapes.

Figure 3: *2D images of the 3D shapes.*

Digital phantoms extracted from patient images

Planning CT Images were used in this retrospective study. Digital phantoms were created by extracting the liver, heart, spinal cord, kidneys and body based on the contours as shown in figure 4. Bulk densities of 60, 40, 15, 20, -200, 0 and 80 HU were then assigned to the liver, heart, spinal cord, kidneys, lungs, body and target respectively.

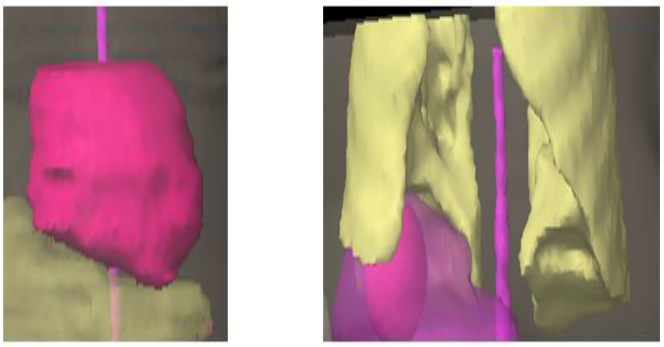

Figure 4: *3D views of the heart and the lungs extracted from patient.*

Geometric inaccuracy simulation

For each digital phantom, MR geometric inaccuracy was simulated by generating distorted images based on the calculated distortion map and the blurring artifact. The geometric distortion as well as the blurring artifact viewed by any 3D point will depend on its position related to the target. A Bspline interpolation was used for simulating the distortion while the blur was simulated by convolving original datasets with a Gaussian function with a Full Width at Half Maximum FWHM varying from 2 mm to 4 mm representing the amount of calculated blur.

Treatment planning

Automatic contours where generated on both original and deformed images using thresholding technique provided by EclipseTM Treatment Planning System (TPS). Dual-arc, 6-MV volumetric modulated arc therapy (VMAT) plans were generated and optimized to irradiate the target on the deformed set of images. The treatment isocenter was placed at the center of the target. A dose of 5000 cGy in 5 fractions was prescribed and dose calculations were performed on a rectangular grid of 1 mm3 voxel size.

The plans, optimized on the distorted datasets, were then transferred to the original datasets and the dose distribution was calculated. Dose Volume Histograms (DVH) including the dose received by 95% (D95) and 50% (D50) of the volume, maximum dose Dmax and the mean dose (Dmean) received by the volume, calculated on distorted and original datasets were finally compared and the dosimetric impact of the MR geometric inaccuracy was assessed.

Results

Digital phantoms composed from 3D shapes

Four different digital phantoms composed from 3D shapes were generated; the first digital phantom, shown in figure 5-a, is composed of a spherical target of 7 mm diameter and is surrounded by 3 spheres organ shapes of 5 mm diameters and 1 ellipsoidal organ shape with a width of 6 mm and a height of 5 mm. The second phantom is composed of a C shape target of 5 and 7 mm of inner and outer diameters respectively. This C shape is surrounding a spherical target shape of 5 mm diameter. It is also surrounded by 3 spheres organ shapes of 5 mm

diameters and 1 ellipsoidal organ shape with a width of 6 mm and a height of 5 mm as shown in figure 5-b. Figure 5-c shows the third digital phantom which is composed of a hollow cylindrical target shape of 5 and 7 mm. This target is surrounding a cylindrical organ shape of 3 mm diameter. Another ellipsoidal organ shape with a width of 6 mm and a height of 5 mm is also included. The last phantom, shown in figure 5-d is composed of a hollow semi-cylindrical target shape of 5 and 7 mm. this target is surrounding a cylindrical organ shape of 3 mm diameter. Another ellipsoidal organ shape with a width of 6 mm and a height of 5 mm is also included.

The shapes and dispositions of these 3D volumes allow evaluating

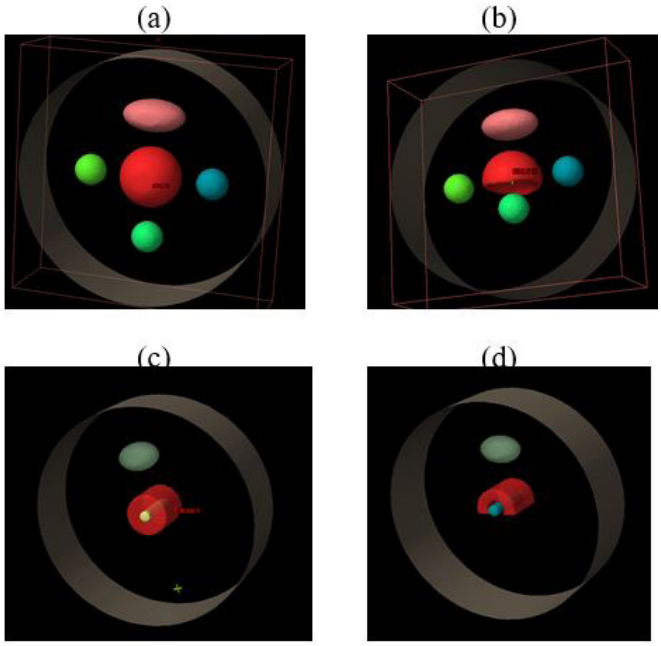

Figure 5:*View of digital phantoms with 3D volumes of different shape and disposition.*

the MR inaccuracy of an external beam treatment within two specific contexts. In the first context, the tumor is surrounded by four OARs in each direction, while in the second; the tumor is surrounding the OAR.

Finally, a dataset of 42 2D DICOM images was generated with a resolution of 512X512 pixels2, a 3 mm slice thickness, a 0 mm gap between slices and a pixel size of 0.97x0.97 mm2 as shown in figure 6.

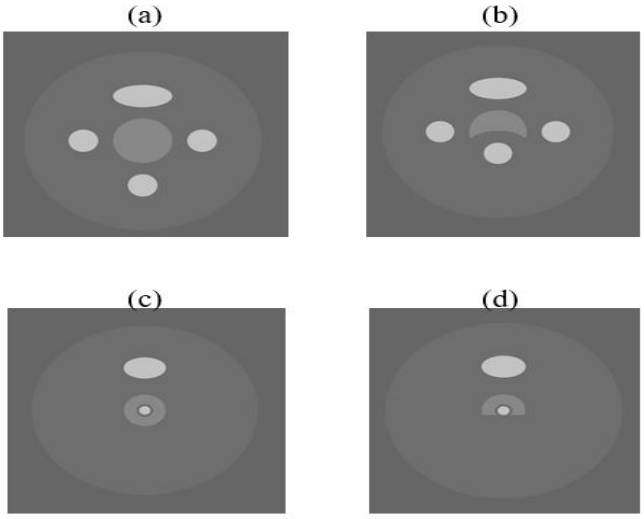

Figure 6: *2D DICOM slices of the four digital phantoms.*

Digital phantoms extracted from patient images

Planning CT Images of 2 liver cancer patients were used to generate digital phantoms. The first patient contains 150 slices of 3 mm thickness, composed of 512X512 pixels2 and a pixel size of 1.6X1.6 mm2. For this patient, the Liver, heart, spinal cord and kidneys were extracted. The second patient contains 100 slices of 3 mm thickness, composed of 512X512 pixels2 and a pixel size of 1.27X1.24 mm2. For this patient the Liver, heart, spinal cord, kidneys and lungs were extracted as shown in figure 7.

From each digital phantom, four set of images were derived in which spherical targets of 50, 40, 30, 20 and 15 mm of diameter were added respectively. The positions of these targets correspond to the clinical position of the Gross Tumor Volume GTV as shown in figure 7. This procedure allows evaluating the dosimetric impact of MR inaccuracy of an external beam treatment related to the size of the targets.

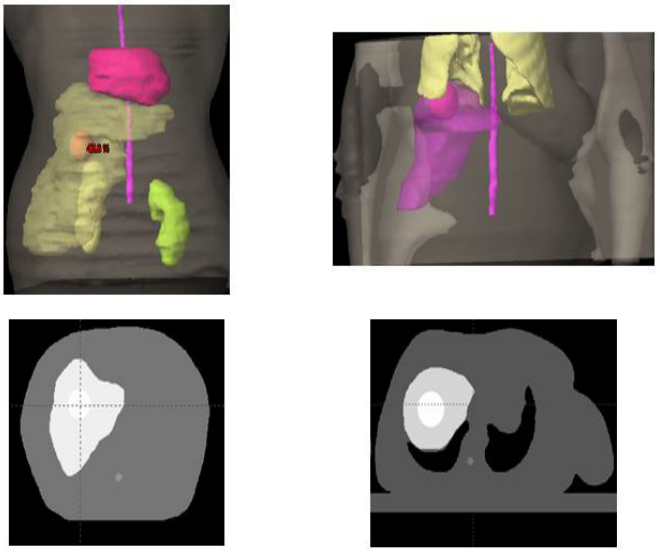

Figure 7: *a) 3D and 2D views of the digital phantoms extracted from a) the first patient and b) the second patient. Liver, heart, spinal cord, kidneys, lungs and the tumor are shown.*

Dosimetric impact of MR inaccuracies on digital phantoms composed from 3D shapes

The mean difference in percent of Dmax, Dmean, D95 and D50 received by the target and the organs at risk are shown in table 2. For the target, these differences were equal to -4.8, -5.6, -6.2 and -5.2% for Dmax, Dmean, D95 and D50 respectively. These values were -6.5, -6.2, -7.2 and -6.8% for the OARs.

Table 2:*Difference in percent of Dmax received by the target.*

Structure	Percentage D_{max} differences	Percentage D_{mean} differences	Percentage D_{95} differences	Percentage D_{50} differences
Target	-4.8	-5.6	-6.2	-5.2
OAR	-6.5	-6.2	-7.2	-6.8

Dosimetric impact of MR inaccuracies on digital phantoms extracted from patients

The mean difference in percent of Dmax, Dmean, D95 and D50 received by the targets of different diameters calculated for the patients are shown in table 3. For a target volume of 50 mm, the mean differences were equal to -0.4, -0.2, 0 and -0.4% for Dmax, Dmean, D95 and D50 respectively. These values ranged between -0.7 to -13.2, -0.3 to -12, -0.1 to -8.2 and -0.5 to -12.7% for target volumes of 40, 30, 20 and 15 mm diameter respectively.

Table 3:*Difference in percent of Dmax received by the target.*

Target diameter	Percentage D_{max} differences	Percentage D_{mean} differences	Percentage D_{95} differences	Percentage D_{50} differences
50 mm	-0.4	-0.2	0	-0.4
40 mm	-0.7	-0.3	-0.1	-0.5
30 mm	-3.1	-3	-2.2	-3.1
20 mm	-7	-6.4	-4.4	-6.7
15 mm	-13.2	-12	-8.2	-12.7

Table 4 shows the mean difference in percent of Dmax and Dmean received by the liver and the spinal cord for targets of different diameters. For the liver, the mean differences for Dmax and Dmean ranged between -0.9 and -15.5% for target volumes of 50, 40, 30, 20 and 15 mm diameter. For the spinal cord, the mean differences for Dmax and Dmean ranged between -0.6 and -20% for target volumes of 50, 40, 30, 20 and 15 mm diameter.

Table 4:*Difference in percent of Dmax and Dmean received by the spinal cord and the liver.*

Target diameter	Percentage D_{max} differences		Percentage D_{mean} differences	
	Liver	Spinal cord	Liver	Spinal cord
50 mm	-2.4	-0.6	-0.9	-3.3
40 mm	-3	-1.3	0	-3.8
30 mm	-5.3	-1.5	-3.9	-3
20 mm	-7.9	-4.9	-3.7	-6.25
15 mm	-15.5	-12.5	-11.7	-20

Discussion

MRI represents a promising technology and alternative to the four-dimensional computed tomography (4D-CT) to assist in volume contouring and to establish motion management strategies for external beam radiation therapy. However, one of the main obstacles to using MR image sets in the design of motion management strategies is the existence of system-related geometric inaccuracies during motion. In this work, we have studied the dosimetric impact in volumetric modulated arc therapy (VMAT) of the MR geometric inaccuracies during motion.

The dosimetric impact of MR geometric inaccuracy for stereotactic radiation therapy has been evaluated and reported in previous studies [34, 35]. In these studies, the MR geometric inaccuracy was represented only by the geometric distortion since the assessment was performed in static mode. In our work, the MR geometric accuracy was assessed during motion and thus represented by the geometric distortion as well as the blurring artifact. As such, this work is the first to evaluate the dosimetric impact of MR geometric inaccuracy during motion.

An MR compatible control point based phantom was used to characterize the geometric accuracy during motion. Compared to static mode, the results showed an increase of the distortion measured during motion on the order of 0.04 mm, 0.24 and 0.3 mm for radial distances of 50, 100 and 150 mm respectively. Regarding the blurring artifact; differences were observed between the phantom in static mode and during motion with an increase of 16% under movements. These results suggested the importance to assess dosimetric impact of the MR geometric inaccuracies during motion especially for regions of interest lying within a relatively large FOV since the magnitude of system related geometric inaccuracies increases with growing radial distance from the scanner's isocenter.

A methodology of generating digital phantoms was developed and presented in this study. Digital phantoms composed of 3D volumes as well as extracted from real patients were used to investigate the dosimetric impact of the MR geometric inaccuracies during motion. Deformed datasets were generated and dose plans were initially generated optimized on these datasets and transferred to the original datasets for comparison. The application of this methodology showed that, due to the sharp dose fall-off at the edge of target, the VMAT plans used with SBRT are sensitive to spatial errors. As such, the evaluation of the dosimetric impact of these inaccuracies, especially for small shapes, represents an essential step for ensuring the effectiveness of the radiation treatment.

Our results showed also that for both target and OAR, the dose received by the original set of images (not deformed) is higher than the dose received by the distorted images on which the plan was initially optimized. For the digital phantoms composed of 3D shapes, the dose percentage is 6 % higher, and for digital phantoms extracted from real patients, the dose percentage is 5.6 % higher. This can be explained by the fact that the blurring artifact is expanding the target and the OAR. As such the treatment plan created on the distorted set of images will cover larger volumes compared to original organs.

These results showed also that the dosimetric impact is inversely proportional to the size of the target. A higher dosimetric impact on the target, the liver and the spinal cord was observed for smaller targets as shown in figure 8 and figure 9.

Although the number of digital phantoms used in this study was small, this is the first study, to our knowledge, to assess the dosimetric impact of MR inaccuracies during motion. Further data will be collected and more investigations will be conducted to confirm this finding.

Finally, the methodology used in this study, which is based on digital

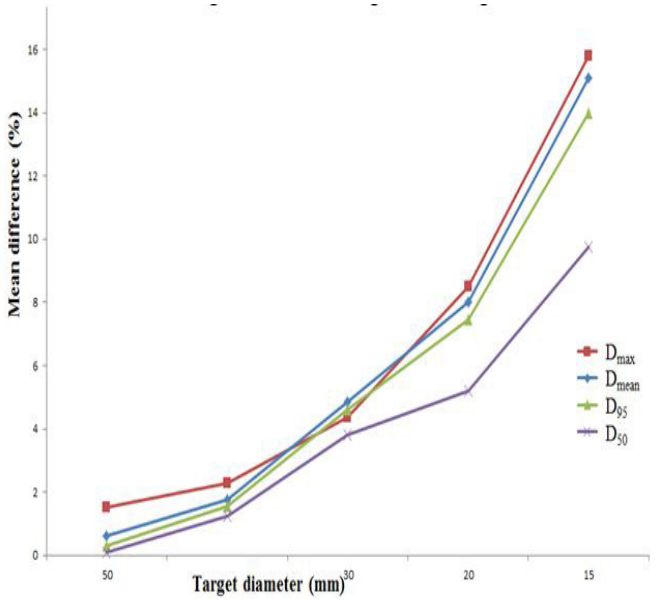

Figure 8: *a) Dosimetric impact of MR inaccuracy on the target relative to the size of the target.*

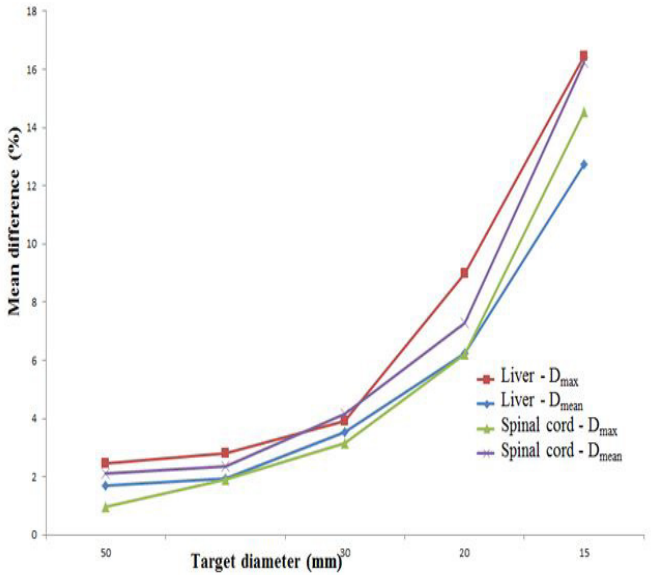

Figure 8: *a) Dosimetric impact of MR inaccuracy on liver and the spinal cord relative to the size of the target.*

phantoms, represents an important technique allowing the assessment of the dosimetric impact of organ deformation for different anatomic sites as well as different treatment techniques. Based on this methodology, the authors are planning to extend this work in order to study the dosimetric impact of MR inaccuracies on different treatment planning techniques such as brachytherapy and Cyberknife.

Conclusion

A methodology of generating digital phantoms was developed and presented in this study. Based on different type of digital phantoms, the dosimetric impact of MRI inaccuracies during motion on liver SBRT plans was analyzed.

Our preliminary results showed that DVH metrics were affected by up to 15% for small size targets.

The methodology used in this study, represents an important technique allowing the assessment of the dosimetric impact of organ deformation for different anatomic sites as well as treatment techniques. Further data will be generated and more investigations will be conducted to confirm our findings and to study the dosimetric impact of MR inaccuracies on different treatment planning techniques.

Conflict of interest

No conflicts of interest.

Reference

1. Potters L., Kavanagh B., Galvin J.M., Hevezi J.M., Janjan N.A., Larson D.A., Mehta M.P., Ryu S., Steinberg M., Timmerman R., et al. American Society for Therapeutic Radiology and Oncology (ASTRO) and American College of Radiology (ACR) Practice Guideline for the Performance of Stereotactic Body Radiation Therapy. Int. J. Radiat. Oncol. Biol. Phys. 2010; 76:326–332.
2. Timmerman RD, Herman J, Cho LC. Emergence of stereotactic body radiation therapy and its impact on current and future clinical practice. J Clin Oncol. 2014; 32:2847–2854.
3. Liu E., Stenmark M.H., Schipper M.J. Stereotactic body radiation therapy for primary and metastatic liver tumors. Transl Oncol. 2013; 6:442–446.
4. Herfarth K.K., Debus J., Lohr F. Stereotactic single-dose radiation therapy of liver tumors: Results of a phase I/II trial. J Clin Oncol. 2001; 19:164–170.
5. Rusthoven K.E., Kavanagh B.D., Cardenes H. Multi-institutional phase I/II trial of stereotactic body radiation therapy for liver metastases. J Clin Oncol. 2009; 27:1572–1578.
6. Schmidt MA, Payne GS. Radiotherapy planning using MRI. Phys Med Biol. 2015;60(22):R323-61
7. Nyholm T, Jonsson J. Counterpoint: opportunities and challenges of a magnetic resonance imaging–only radiotherapy work flow. Semin Radiat Oncol. 2014;24:175-80.
8. Kupelian P, Sonke JJ. Magnetic resonance-guided adaptive radio-therapy: A solution to the future.Semin Radiat Oncol2014;24:227-232.
9. Persson E, Gustafsson C, Nordstrom F, et al. MR-OPERA: a multicenter/multivendor validation of magnetic resonance imaging-only prostate treatment planning using synthetic computed tomography images. Int J Radiat Oncol Biol Phys. 2017;99:692–700.
10. Lee YK, Bollet M, Charles-Edwards G, Flower MA, Leach MO, McNair H, Moore E, Rowbottom C, Webb S. Radiotherapy treatment planning of prostate cancer using magnetic resonance imaging alone. Radiother Oncol 2003;66:203-16.
11. Cai J, Chang Z, Wang Z, Paul Segars W, Yin FF. Four-dimensional magnetic resonance imaging (4D-MRI) using image-based respiratory surrogate: a feasibility study. Med Phys. 2011;38:6384–6394.
12. Yang J, Cai J, Wang H, et al. Four-dimensional magnetic resonance imaging using axial body area as respiratory surrogate: initial patient results. Int J Radiat Oncol Biol Phys. 2014;88:907–912.
13. Hu Y, Caruthers SD, Low DA, Parikh PJ, Mutic S. Respiratory amplitude guided 4-dimensional magnetic resonance imaging. Int J Radiat Oncol Biol Phys. 2013;86:198–204.
14. Kubo HD, Hill BC. Respiration gated radiotherapy treatment: a technical study. Phys Med Biol. 1996;41:83–91.
15. Nelson C, Starkschall G, Balter P, et al. Respiration-correlated treatment delivery using feedback-guided breath hold: a technical study. Med Phys. 2005;32:175–181.
16. Kini VR, Vedam SS, Keall PJ, Patil S, Chen C, Mohan R. Patient training in respiratory-gated radiotherapy. Med Dosim. 2003;28:7–11.
17. Tryggestad E, Flammang A, Han-Oh S, et al. Respiration-based sorting of dynamic MRI to derive representative 4D-MRI for radiotherapy planning. Med Phys. 2013;40:051909.
18. Liu Y, Yin FF, Chang Z, et al. Investigation of sagittal image acquisition for 4D-MRI with body area as respiratory surrogate. Med Phys. 2014;41:101902.
19. Han F, Zhou Z, Cao M, Yang Y, Sheng K, Hu P. Respiratory motion resolved, self-gated 4D-MRI using rotating cartesian k-space (ROCK). Med Phys. 2017;44:1359–1368
20. Stanescu T, Jans HS, Wachowicz K, Fallone BG. Investigation of a 3D system distortion correction method for MR images. J Appl Clin Med Phys. 2010;11:2961.
21. Torfeh T, Hammoud R, McGarry M, Al-Hammadi N, Perkins G. Development and validation of a novel large field of view phan-

tom and a software module for the quality assurance of geometric distortion in magnetic resonance imaging. Magn Reson Imaging. 2015;33:939–949.

22. Torfeh T, Hammoud R, Perkins G, et al. Characterization of 3D geometric distortion of magnetic resonance imaging scanners commissioned for radiation therapy planning. Magn Reson Imaging. 2016;34:645–653.
23. Walker A, Liney G, Metcalfe P, Holloway L. MRI distortion: considerations for MRI based radiotherapy treatment planning. Australas Phys Eng Sci Med. 2014;37:103–113.
24. Wang D, Strugnell W, Cowin G, Doddrell DM, Slaughter R. Geometric distortion in clinical MRI systems Part I: evaluation using a 3D phantom. Magn Reson Imaging. 2004;22:1211–1221.
25. Doran SJ, Charles-Edwards L, Reinsberg SA, Leach MO. A complete distortion correction for MR images: I. Gradient warp correction. Phys Med Biol. 2005;50:1343–1361.
26. Huang KC, Cao Y, Baharom U, Balter JM. Phantom-based characterization of distortion on a magnetic resonance imaging simulator for radiation oncology. Phys Med Biol. 2016;61:774–790.
27. Baldwin LN, Wachowicz K, Fallone BG. A two-step scheme for distortion rectification of magnetic resonance images. Med Phys. 2009;36:3917–3926.
28. Price RG, Knight RA, Hwang K, et al. Optimization of a novel large field of view distortion phantom for Mr-only treatment planning. J Appl Clin Med Phys. 2017;18:51–61.
29. Baldwin LN, Wachowicz K, Thomas SD, Rivest R, Fallone BG. Characterization, prediction, and correction of geometric distortion in 3 T MR images. Med Phys. 2007;34:388–399.
30. Adjeiwaah M, Bylund M, Lundman JA, et al. Quantifying the effect of 3T magnetic resonance imaging residual system distortions and patient-induced susceptibility distortions on radiation therapy treatment planning for prostate Cancer. Int J Radiat Oncol Biol Phys. 2018;100:317–24.
31. Liney GP, Owen SC, Beaumont AK, Lazar VR, Manton DJ, Beavis AW. Commissioning of a new wide-bore MRI scanner for radiotherapy planning of head and neck cancer. Br J Radiol. 2013;1027:20130150.
32. Gustafsson C, Nordström F, Persson E, et al. Assessment of dosimetric impact of system specific geometric distortion in an MRI only based radiotherapy workflow for prostate. Phys Med Biol. 2017;62:2976–2989.
33. Walker, A., Metcalfe, P., Liney, G. et al. MRI geometric distortion: Impact on tangential whole-breast IMRT. J Appl Clin Med Phys. 2016; 17: 7–19
34. Pappas EP, Alshanqity M, Moutsatsos A, et al. MRI-Related Geometric Distortions in Stereotactic Radiotherapy Treatment Planning: Evaluation and Dosimetric Impact. Technol Cancer Res Treat. 2017;16(6):1120-1129.
35. Han S, Yin FF, Cai J. Evaluation of dosimetric uncertainty caused by MR geometric distortion in MRI-based liver SBRT treatment planning. J Appl Clin Med Phys. 2019;20(2):43-50.
36. Torfeh T, Hammoud R, El Kaissi T, et al. Geometric accuracy of the MR imaging techniques in the presence of motion. J Appl Clin Med Phys. 2018;19(2):168-175.